DESIGN AND EXPERIMENT OF AN AIR-ASSISTED, GUIDED-GROOVE MAIZE SEED-GUIDING DEVICE BASED ON THE BRACHISTOCHRONE CURVE

/

基于最速降线的气辅-导槽式玉米导种装置设计与试验

Wen-sheng SUN [1)], Shu-juan YI[*1)], Hai-long QI [2)], Yi-fei LI [1,3)], Yu-peng ZHANG [1)], Jia-sha YUAN [1)], Song WANG [1)]
[1)]College of Engineering, Heilongjiang Bayi Agricultural University, Daqing/P.R.China
[2)]Heilongjiang Beidahuang Modern Agricultural Service Group Zhongrong Agricultural Machinery Co., Ltd, Harbin / P.R.China
[3)]College of Engineering, Northeast Agricultural University, Harbin/P.R.China
Tel: +86-459-13836961877; E-mail: yishujuan_2005@126.com
Corresponding author: Shu-juan Yi
DOI: https://doi.org/10.35633/inmateh-76-19

ABSTRACT

To address the issue that existing seed-guiding devices struggle to meet the high-speed operational requirements of delta-row planters for dense maize planting, a seed-guiding device with air assistance and a guided groove was designed based on the principle of the brachistochrone. The overall structure and working principle of the device are described, and the curved segment of the seed guide tube was optimized using the brachistochrone principle while accounting for frictional effects. Computational fluid dynamics (CFD) simulations were conducted to analyse the flow field characteristics of the seed guide tube at inlet airflow velocities of 63.48, 60.64, 57.73, 54.69, 51.50, and 48.15 m/s. A multi-factor test was performed using chamber pressure and operating speed as test factors, with the qualified index of grain spacing and the coefficient of variation as evaluation metrics. Comparative tests were conducted using a traditional guided-groove seed guide tube and a brachistochrone-based seed guide tube without a guided groove. Results showed that the optimal parameter combination for the newly designed device was a chamber pressure of 3.124 kPa and an operating speed of 12.0 km/h. Under these conditions in the bench test, the qualified index reached 97.04%, and the coefficient of variation was 6.18%, outperforming the other two types of seed-guiding devices. These findings demonstrate that the seed-guiding device based on the brachistochrone principle can significantly improve the seeding quality of delta-row planters for dense maize planting under high-speed operation.

摘要

针对现有导种装置难以满足玉米品字形密植播种机高速作业需求的问题，基于最速降线原理设计了一种气辅-导槽式导种装置。阐述了导种装置的总体结构与工作原理，根据考虑摩擦力下的最速降线原理对导种管曲线段进行了优化设计，得到了曲线段轮廓的解析方程。通过 CFD 仿真试验探究了导种管在入口流速分别为 63.48、60.64、57.73、54.69、51.50、48.15m/s 时的流场特性。以腔室压力与作业速度为试验因素，以粒距合格指数、粒距变异系数为试验指标开展了多因素试验，确定了导种装置最优参数组合并对其进行了试验验证，同时开展了与传统导槽式导种装置、无导槽最速降线式导种装置的对比试验。结果表明：该导种装置的最优工作参数组合为腔室压力 3.124 kPa、作业速度 12.0 km/h，台架验证该参数组合下的粒距合格指数为 97.04%、粒距变异系数为 6.18%，并且较另外两种导种装置表现出了更优的导种性能，说明基于最速降线原理设计的气辅-导槽式导种装置可以进一步提高玉米密植播种机在高速作业条件下的播种质量。

INTRODUCTION

　　Maize precision planting refers to the process of sowing single maize seeds into a predetermined soil seedbed position with a precision planter according to the sowing density required by local agronomy, in accordance with consistent row spacing, uniform grain spacing and precise depth *(Zhao et al., 2024; Sun et al., 2024)*.

---

[1]*Wen-sheng Sun, Ph.D.; Shu-juan Yi, Prof. Ph.D.; Hai-long Qi, bachelor degree; Yi-fei Li, Ph.D.; Yu-peng Zhang, master degree; Jia-sha Yuan, master degree; Song Wang, Ph.D.*

The seed-guiding mechanism is one of the final links in the maize precision planting process, ensuring that seeds enter the soil in a uniform and orderly manner. It not only maintains the orderly state of seeds achieved in the preceding steps but also directly influences the uniformity of seed distribution in the field *(Yatskul et al., 2018; Liao et al., 2020)*. However, the random movement of maize seeds from the seed-metering device into the seed-guiding unit, combined with collisions within the guide, disrupts the smooth flow of seeds. This results in deviations from the intended placement in the seedbed, ultimately reducing sowing quality.

Extensive research has been carried out by agricultural machinery companies and researchers to address the issue of maize seed misplacement caused by collisions during the seed-guiding process. The U.S.-based company Precision Planting developed a belt-type seed-guiding device that uses a conveyor belt to transport maize seeds from the seed-metering device to the seed outlet. By matching the conveyor speed with the planter's operating speed, the system ensures consistent seed spacing under varying operating conditions. The Swedish company Vaderstad introduced an airflow-projection seed-guiding device, which utilizes positive pressure airflow to constrain and rapidly project seeds into the soil through a seed guide tube, enabling high-speed maize planting. *Dong Jianxin et al., (2023),* designed a guided seed-casting mechanism that optimizes the seed guide trajectory, enhancing the seed placement accuracy of attitude-controlled drive-guided seed-metering devices under high-speed conditions. *Li Yuhuan et al. (2020)* achieved linear seed-throwing of maize under high-speed conditions by incorporating a seed-pushing mechanism into an air-suction high-speed precision seed-metering device, in coordination with specially shaped holes on the seed-metering plates. *Liu Rui et al. (2023)* designed a seed-guiding device based on the Venturi principle, utilizing positive pressure airflow assistance to effectively address the issue of seeds failing to enter the seedbed in an orderly, single-grain manner due to violent collisions. The brachistochrone theory, which addresses the optimization of velocity and path selection *(Adetifa et al., 2021)*, has also been applied in the optimal design of curved structures in agricultural machinery components. *Tang Han et al. (2023)* applied the brachistochrone theory to the structural design of the curved section of the seed guide tube in an internally-filled, air-blowing seed-metering device. Bench tests showed that, under a working pressure of 4.5 kPa and a working speed of 41 r/min, the seed spacing qualified index and the coefficient of variation reached 96.56% and 9.58%, respectively. Similarly, *Jia Xian et al. (2024)* optimized the seed-guiding curve of a gravity-type seed guide tube based on the brachistochrone principle. Bench test results indicated that the coefficient of variation was reduced by approximately 3% compared to that of a traditional gravity-type seed guide tube within the operating speed range of 9.0 to 14.4 km/h. However, due to the high installation precision and compatibility required between the seed-guiding device and the seed-metering unit, current seed-guiding devices struggle to meet the operational demands of high-speed delta-row planters for dense maize planting.

To improve the seeding quality of high-speed delta-row planters for dense maize planting, a seed-guiding device with air assistance and a guided-groove structure was designed based on the principle of the brachistochrone. The curved segments of the seed guide tube were optimized using the brachistochrone curve while accounting for friction, and were combined with a guided-groove structure to constrain seed movement under high-speed positive pressure airflow. This study provides a technical reference for enhancing the performance of seed-guiding devices in high-speed planters for dense maize planting.

MATERIALS AND METHODS

Overall structure and working principle

As shown in Fig. 1, the seed-guiding device primarily consists of a pressure relief wheel and its connecting frame, a seed-discharge tube, a transition tube, a seed guide tube, and suppression wheels. To coordinate with the seed discharge operation of the seed-metering device *(Sun et al., 2024)*, key components such as the pressure relief wheels, seed-discharge tube, transition tube, seed guide tube, and suppression wheels are symmetrically arranged. Two identical pressure relief wheels are installed inside the corresponding shaped holes at the seed-unloading points of the two seed-metering plates. These wheels serve to block airflow and ensure that seeds are smoothly discharged from the plates into the seed-discharge tube. To maintain the sealing integrity of the air-pressure seed-metering system and to allow smooth transfer of seeds detached from the plates, the seed-discharge tube is integrated into the device shell. The transition tube serves to connect the seed-discharge tube with the seed guide tube.

As the core working part of the whole seed-guiding device, the seed guide tube consists of linear and curved segments, and the upper and lower combined guided-groove structures are set to produce a restraining

effect on the movement of the seeds passing through the seed guide tube. The key structural parameters of the seed guide tube *(Yi et al., 2025)*, such as the outer diameter d_1 of the tube body is 21 mm, the inner diameter d_2 of the tube body is 17 mm, the length L_1 of the seed guide tube is 550 mm, the width H_1 is 100 mm, the length L_2 of the linear section is 310 mm, the length L_3 of the curved section is 240 mm, the guided-groove height L_4 is 355 mm, the width w_1 of the upper guided-groove is 1.3 mm, the width w_2 of the lower guided-groove is 2.2 mm. According to the agronomic requirements of narrow-wide-row delta-row dense planting area of maize in Heilongjiang province, the spacing L of narrow-single-row is 18~20 cm, the spacing L_0 of narrow-double-row is half of the spacing L, and the spacing H of narrow-row is 13 cm. Therefore, the row spacing of the two seed guide tubes is 13 cm.

The seed-guiding device can be divided into three functional zones based on the working process: the seed-delivery zone, the seed-attracting zone, and the seed-attaching zone. After the seed-metering device delivers seeds to the seed-unloading points, the pressure relief wheel blocks the inner side of the corresponding holes at these points, causing the seeds to lose the pressure attachment force. As a result, the seeds enter the seed-delivery zone vertically under the combined action of gravity and airflow. Within the seed-delivery zone, seeds sequentially pass through the seed-discharge tube, the transition tube, and the straight segment of the seed guide tube, accelerating as they fall. When the seeds enter the seed-attracting zone, a pressure difference is generated between the inside and outside of the tube due to the influence of the guided-groove structure. This pressure difference creates an additional pressure field that causes the seeds to move toward the end of the seed guide tube while simultaneously shifting toward the guided groove under the action of this pressure field. Once the seed is stably attached to the guided groove, it enters the seed-attaching zone, where it moves along the inner sidewall of the groove toward the seed-throwing point under the combined forces of gravity, airflow, and friction. Finally, the seed exits the seed guide tube at the seed-throwing point and is pressed into its predetermined position in the seedbed by the suppression wheels, completing the seed-guiding process. Through the staggered discharge timing of the seed-metering device and the orderly regulation provided by the seed-guiding device, maize seeds are accurately placed in the seedbed to form a narrow-row, delta-row sowing pattern.
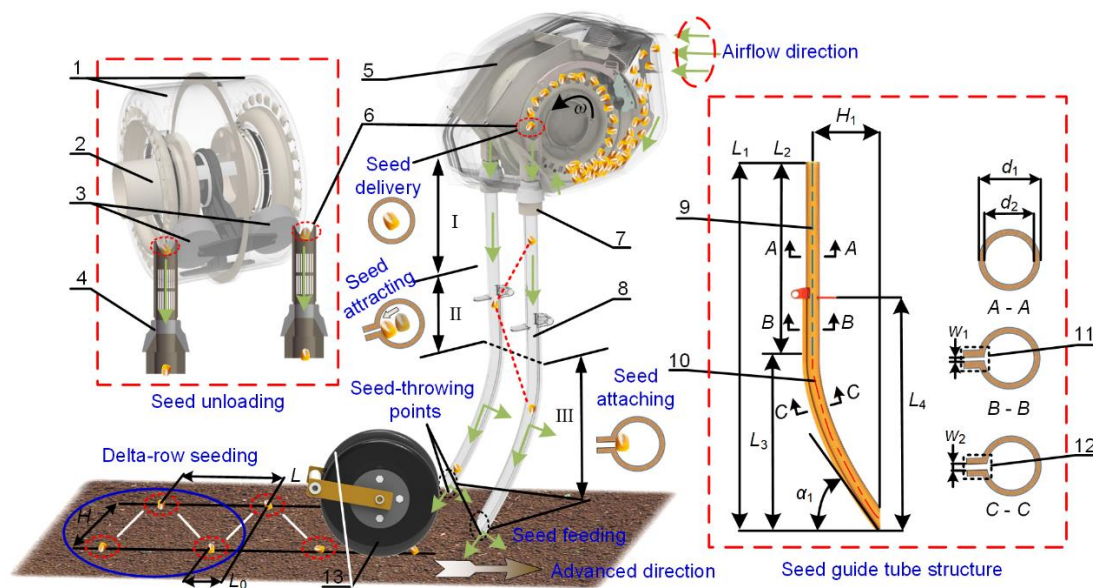

Fig. 1 - Overall structure and working principle
1. seed-metering plates; 2. connecting frame; 3. pressure relief wheel; 4. seed-discharge tube; 5. seed-metering device;
6. seed-unloading point; 7. transition tube; 8. seed guide tube; 9. linear segment; 10. curved segment; 11. upper guided-groove;
12. lower guided-groove; 13. suppression wheels; I. seed-delivery zone; II. seed-attracting zone; III. seed-attaching zone.

Design of curved segments of the seed guide tubes

Under high-speed operating conditions of planters for dense maize planting, the movement of seeds upon detachment from the seed-metering plates becomes highly random. This increased randomness leads to a higher frequency of seed collisions within the seed-guiding device, ultimately reducing seeding uniformity *(Fanigliulo et al., 2022; Ma et al., 2023)*.

Studies have shown *(Li et al., 2023)* that the curve structure designed based on the principle of the brachistochrone is conducive to the improvement of irregular seed mobility and seed-throwing uniformity.

Therefore, in this study, the structural design of the curved segments of the seed guide tubes was carried out based on the principle of the brachistochrone.

As shown in Fig. 2, according to the principle of the brachistochrone, the equation of the curve trajectory (l_1) that takes the shortest time for the maize seed to go from point A to point B when friction is not considered is:

$$\begin{cases} x = R_1\left(\dfrac{\pi\theta_1}{180} - \sin\theta_1\right) \\ y = R_1(1 - \cos\theta_1) \end{cases} \tag{1}$$

where:

R_1 is the radius of the circle in the *Axy* coordinate system, m; θ_1 is the rolling angle of rotation of the circle in the *Axy* coordinate system, (°).
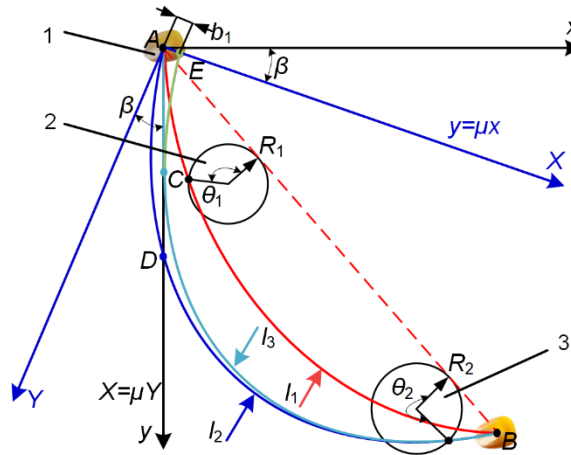

Fig. 2 - Schematic diagram of the combined brachistochrone curve
1. maize; 2. circle in the Axy coordinate system; 3. circle in the AXY coordinate system.

The velocity v_1 at any point during the fall of the seed is:

$$v_1 = \frac{ds}{dt} = \frac{\sqrt{1 + y'^2}}{dt}dx \tag{2}$$

where:

s is the length of any curve arc, m; t is the time, s; y' is the first-order derivative of the curve trajectory equation.

Assuming that the seed slides tightly against the surface without bouncing, the angle φ of the seed during the fall tends to zero. After considering friction, the change ΔE in kinetic energy of the seed during its descent from point A according to the kinetic energy theorem is:

$$\Delta E = d\left(\frac{1}{2}mv_1^2\right) = mgdy - \mu mg\cos\varphi ds \Rightarrow v_1 = \sqrt{2g(y - \mu x)} \tag{3}$$

where:

m is the mass of the seed, m; g is the acceleration of gravity, m/s²; μ is the rolling friction coefficient between the maize seed and the seed guide device; φ is the angle between the normal direction of the seed's location and the vertical direction, (°); x, y are the coordinates of the seed's position in the *Axy* coordinate system, m.

The time T taken by the seed to travel from point A to point B can be expressed as:

$$T = \int dt = \int_0^{x_B} \frac{\sqrt{1 + y'^2}dx}{\sqrt{2g(y - \mu x)}} \tag{4}$$

Eq. (4) is solved by rotating the *Axy* coordinate system clockwise by an angle β to obtain the *AXY* coordinate system under friction, and:

$$\beta = \arctan\mu \tag{5}$$

$$y - \mu x = \frac{Y}{\cos\beta} \tag{6}$$

Eq. (4) is then transformed into:

$$T = \int_0^{x_B} \sqrt{\frac{(1 + Y'^2)\cos\beta}{2gY}}\,dX \tag{7}$$

where:

x_B is the horizontal coordinate of point B, m.

However, from Fig. 2, it can be seen that the curve AD (l_2) enters the $x<0$ region, and the velocity of the seed at point D is less than its free fall velocity from point A, indicating that the curve AD is not the optimal path. When the brachistochrone curve is translated from point A to point E along the direction of the X-axis, the seed falls from point A to point C along the boundary $X = \mu Y$, and then along the curve CB to point B, the time T used is:

$$T = \sqrt{\frac{2y_C}{g}} + \int_0^{x_B} \frac{\sqrt{1 + y'^2}\,dx}{\sqrt{2g(y - \mu x)}} \tag{8}$$

where:

y_C is the longitudinal coordinate of point C, m.

But the position of point C is not fixed, and there may be changes when it occurs:

$$\delta T = \frac{1}{\sqrt{2gy_C}}\left(1 - \frac{y'}{\sqrt{1 + y'^2}}\right)\delta y_C \tag{9}$$

When the time T takes the minimum value, the point C needs to satisfy the condition:

$$\begin{cases} \delta T = 0 \\ y' = \infty \end{cases} \tag{10}$$

At this time, the brachistochrone curve CB is tangent to the y-axis, and its trajectory equation in the AXY coordinate system is:

$$\begin{cases} X = R_2\left(\dfrac{\pi\theta_2}{180} - \sin\theta_2\right) + b_1 \\ Y = R_2(1 - \cos\theta_2) \end{cases} \tag{11}$$

where: X, Y is the position coordinate of the AXY coordinate system, m; R_2 is the radius of the circle in the AXY coordinate system, m; θ_2 is the rolling angle of rotation of the circle in the AXY coordinate system, (°); b_1 is the amount of translation of the brachistochrone curve along the X-axis direction, m.

Also, the coordinates of point C satisfy the following conditions:

$$\begin{cases} X_C = R_2\left(\dfrac{\pi\theta_C}{180} - \sin\theta_C\right) + b_1 \\ Y_C = R_2(1 - \cos\theta_C) \\ X_C = \mu Y_C \\ \left.\dfrac{dX}{dY}\right|_C = \dfrac{1 - \cos\theta_C}{\sin\theta_C} = \mu \end{cases} \tag{12}$$

where: X_C, Y_C is the positional coordinate of point C in the AXY coordinate system, m; θ_C is the rolling angle of rotation of the circle in point C, (°).

Obtained from Eq. (12):

$$\mu = \tan\frac{\theta_C}{2} = \tan\beta \tag{13}$$

And then there's:

$$b_1 = R_2(2\mu - 2\arctan\mu) \tag{14}$$

The μ is 0.0931 *(Sun et al., 2024)*, and substituting into Eq. (13) yields θ_C of 10.64° and β of 5.32°, and then substituting into Eq. (14) yields b_1/R_2 = 5×10⁻⁴. According to the above dimensional parameters of the seed guide tube, the coordinates of the point A in the Axy coordinate system are (0, 0), and the coordinates of the point B are (0.1, 0.24). According to the coordinate transformation formula:

$$\begin{bmatrix} X \\ Y \end{bmatrix} = \begin{bmatrix} \cos\beta & \sin\beta \\ -\sin\beta & \cos\beta \end{bmatrix}\begin{bmatrix} x \\ y \end{bmatrix} \tag{15}$$

the coordinates of point A in the AXY coordinate system are found to be (0, 0) and the coordinates of point B are (0.122, 0.230). Substituting the coordinates of point B in the AXY coordinate system and b_1/R_2 = 5×10⁻⁴ into Eq. (11) yields the rolling angle θ_B at point B as 84.45°, R_2 as 0.255, and b_1 as 1.27 × 10⁻⁴. The analytical equation (l_3) for the combined brachistochrone curve AB considering friction is obtained as:

$$\begin{cases} AC: Y = 10.74X \\ CB: \begin{cases} X = 0.255 \times \left(\dfrac{\pi\theta_2}{180} - \sin\theta_2\right) + 1.27 \times 10^{-4} \\ Y = 0.255 \times (1 - \cos\theta_2) \end{cases} \end{cases} \tag{16}$$

By substituting θ_C into Eq. (16), the coordinates of point C in the AXY coordinate system are calculated as (4×10^4, 4×10^{-3}), and the value range of the θ_2 is 10.64~84.45°. Based on the analytical equation (l_3), the curve corresponding to the seed guide tube trajectory was plotted, as shown in Fig. 3. The curved segment of the seed guide tube was then designed in accordance with this trajectory equation.
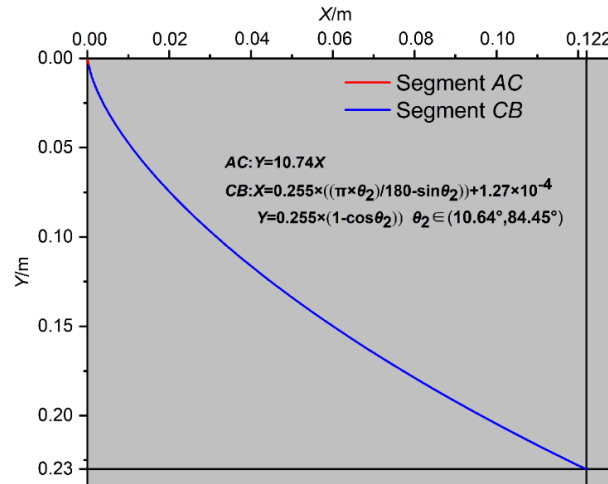

Fig. 3 - Schematic diagram of the outline of the curved section of the seed guide tube

Simulation tests

As shown in Fig. 4, the fluid domain of the seed guide tube is extracted by Space Claim software, and the inlet and outlet of the tube are labelled as "Inlet" and "Outlet", respectively. The labelled model is imported into Fluent Meshing module for meshing. In order to improve the mesh quality of the model, the minimum and maximum values of the surface mesh size were set to 0.5 and 1.5 mm, respectively, and the poly mesh was used for volume mesh-filling. The meshed model is imported into the Fluent solver module, and the widely used standard K-epsilon turbulence model is selected for the simulation. In the Solution Methods, the second-order equations are used for the pressure and momentum equations and the first-order upwind equations are used for the turbulent kinetic energy and turbulent dissipation rate equations. In the Run calculation, the time-step is set to be 1×10^{-2} s, and the total simulation time is set to be 2 s. According to the repeated test results of the actual experiment, the flow velocity v_r of the Inlet was set as 63. 48, 60.64, 57.73, 54.69, 51.50 and 48.15 m/s, respectively, and the pressure of the Outlet was set as 0 Pa to carry out the single-factor simulation experiment, so as to explore the flow field characteristics in the seed guide tube under different inlet velocities.
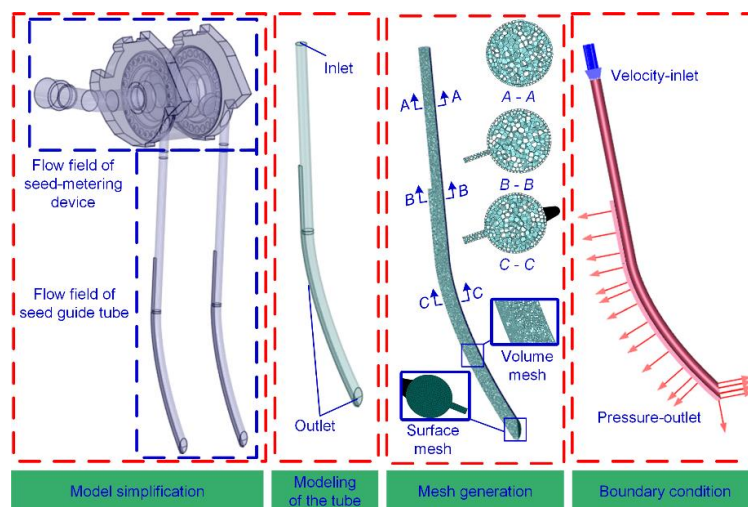

Fig. 4 - Establishment of CFD simulations

Bench tests

In order to determine the optimal working parameter combination of the seed guide device based on the principle of the brachistochrone, and to check its performance improvement effect compared with the traditional seed guide tube with guided-groove and the seed guide tube without guided-groove based on the brachistochrone, the bench performance test was carried out in the High-speed Precision Sowing Lab of the College of Engineering, Heilongjiang Bayi Agricultural University at an ambient temperature of about 20°C and a seed bed oil belt temperature of about 25°C. The test conditions and seeding effect are shown in Fig. 5, and the main devices include seed-supply device, air-pressure seed-metering device, HTB multi-stage blower (Shanghai Liangjin Electromechanical Equipment Co., Ltd, Shanghai), JPS-16 seed-metering device test bench (Heilongjiang Agricultural Machinery Engineering Research Institute, Harbin, Heilongjiang, Mean error of grain spacing measurement ≤2 mm), frequency converter, DP2000 intelligent pressure and wind velocity air volume meter (Shanghai YIOU Instrument Equipment Co., Ltd, Shanghai, resolution 1Pa), as well as three types of seed guide tubes. Among them, the JPS-16 test bench can collect the seed grain spacing falling on the surface of the seed bed oil belt after sowing through computer vision technology, and output the statistical results of the detection indexes using the image acquisition and processing system. The typical maize variety "Dika C2235" planted in Heilongjiang region of China was used for the test seed *(Sun et al., 2024)*, and the related material characteristics are shown in Table 1.
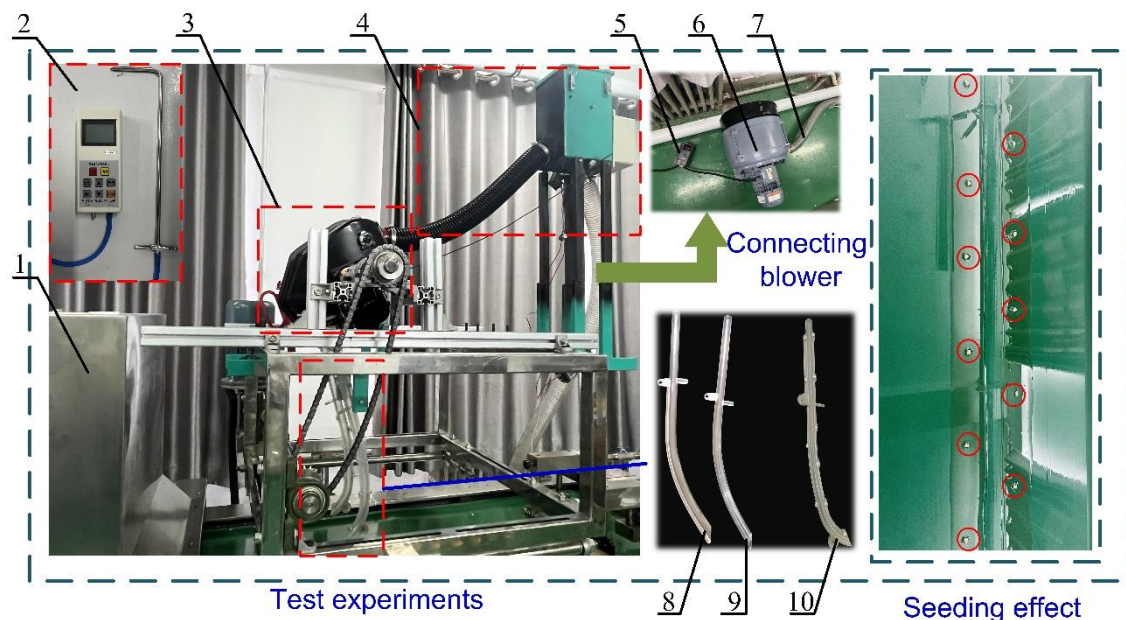

Fig. 5 - Bench test
1. JPS-16 seed-metering device test bench; 2. DP2000 intelligent pressure and wind velocity air volume meter;
3. seed-metering device; 4. seed-supply device; 5. frequency converter; 6. HTB-multi-stage blower; 7. threaded pipe;
8. traditional seed guide tube with guided-groove; 9. seed guide tube without guided-groove based on the brachistochrone;
10. seed guide tube with guided-groove based on the brachistochrone.

Table 1

Basic material characteristics of maize seed

Types	Seed picture	Moisture content / %	Thousand grain weigh / g	Density / g·cm⁻³	Pile angle/(°)	Length/mm	Width / mm	Thickness / mm
Dika C2235 (big-rounded)		12.4	342.3	1.198	22.42	10.24±0.59	9.74±0.54	7.24±0.61

Based on the actual test conditions, the chamber pressure P_f of the seed-metering device was set in the range of 2.7~4.2kPa, and the operating speed v_p was set in the range of 12.0~16.0 km/h. A two-factor, five-level multi-factor experiment was conducted. The coding of the test factors is shown in Table 2, where $X1$ and $X2$ represent the coded values of chamber pressure P_f and operating speed v_p, respectively.

Experimental factors and level codes in multi-factor experiment

Coded values	Experimental factors	
	X1/ kPa	X2/ (km/h)
-1.414	2.70	12.0
-1	2.92	12.6
0	3.45	14.0
1	3.98	15.4
1.414	4.20	16.0

Referring to the international standard ISO 7256/1 (1984) and JB/T10293-2001 "Technical Conditions for Single Grain (Precision) Seeders" *(Tang et al., 2023; Tang et al., 2024)*, the qualified index Q_1 and the coefficient of variation Q_2 were selected as the evaluation indexes of the test, and their calculation formula is as follows:

$$\begin{cases} Q_1 = \dfrac{n_q}{N_1} \times 100\% \\ Q_2 = \sqrt{\dfrac{\sum(x - x_p)^2}{(N_1 - 1)x_p^2}} \times 100\% \end{cases} \tag{17}$$

where:

n_q is the number of qualified grain spacing; N_1 is the total number of intervals; x is the grain spacing measured in the test, m; x_p is the average grain spacing measured in the test, m.

The conversion relationship between the working speed n_p of the seed-metering device and the operating speed v_p of the planter is given by:

$$n_p = \frac{60v_p}{ZL} \tag{18}$$

where: Z is the number of the holes in the seed-metering plates.

The test was conducted by randomly counting the 250 consecutive seed grain spacings adjacent to the sown homogeneous section, and each set of test was replicated 5 times to calculate the qualified index Q_1 and the coefficient of variation Q_2 under different treatments.

RESULTS AND DISCUSSIONS

Results of the simulation experiments

As shown in Fig. 6 a, in order to investigate the flow field distribution of the seed guide tube at different inlet flow velocities, the pressures and flow velocities of different lengths H_2 in the negative direction of the *y*-axis from the inlet of the seed guide tube at 2 s were extracted, and the cloud diagrams of the pressures and flow velocities of the axial plane of the seed guide tube in the *z*-axis direction as well as the vertical cross sections at distances of 100 mm, 200 mm, and 300 mm from the inlet of the tube were intercepted, respectively. The pressure and velocity curves for different lengths H_2 at each velocity-inlet of the tube are shown in Fig. 6 b. The results of the pressure and velocity cloud diagrams in the axial plane and the vertical cross sections are shown in Fig. 6 c and Fig. 6 d, respectively.

In Fig. 6 b, it can be seen that along with the increase of the length H_2, the trends of pressure and velocity curves at different velocity-inlets are basically the same. The velocity curve shows a slow upward trend within the range of 0~380 mm from the length H_2, and a rapid decrease followed by a gradual increase and then a gradual decrease within the range of 380~550 mm. The velocity ranges for inlet-velocities of 48.15, 51.50, 54.69, 57.73, 60.64 and 63.48 m/s in the *y*-axis direction were 36.87 ~ 56.23 m/s, 39.85 ~ 60.04 m/s, 42.71 ~ 63.66 m/s, 45.47~ 67.11 m/s, 48.13 ~ 70.41 m/s, and 50.72 ~ 73.63 m/s, respectively. When the length H_2 ranges from 0 to 321 mm, the pressure decreases rapidly at first and then decreases slowly. When the length H_2 ranges from 321 to 550 mm, the pressure generally shows a fluctuating upward trend. As the inlet velocity increases, the maximum pressure differential along the y-axis also increases, with values of 484.11, 546.29, 608.66, 670.80, 732.73, and 795.78 Pa corresponding to the respective inlet velocities listed above.
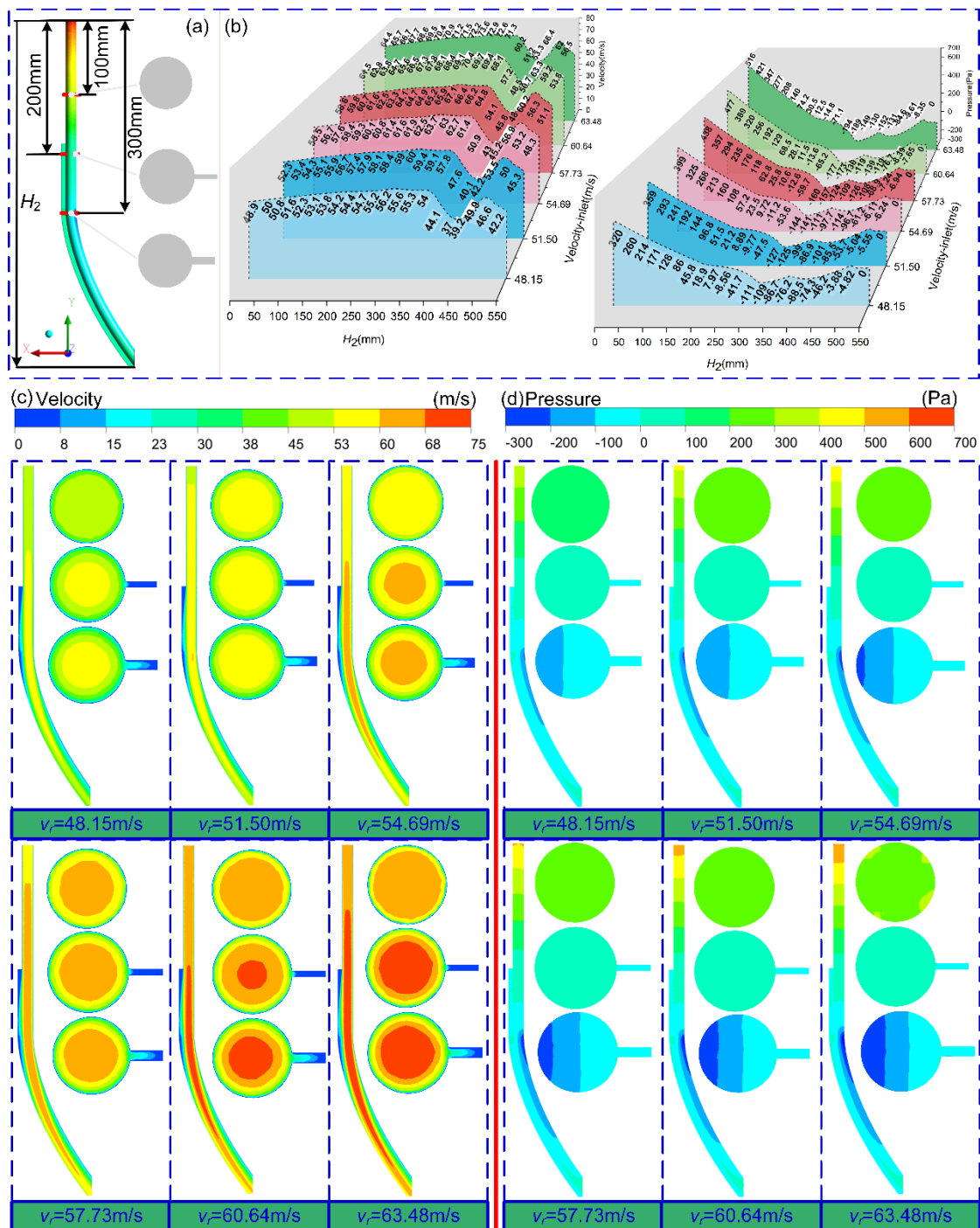
Fig. 6 - Results of CFD simulations

As shown in Fig. 6c, the velocity cloud diagrams in the axial plane reveal that as the inlet velocity increases, the overall flow velocity throughout the flow field also increases. Additionally, the area occupied by the high-velocity zone expands accordingly. However, the increase in flow velocity near the upper guided-groove is less pronounced compared to that observed near the lower guided-groove. Furthermore, the flow velocity near the end of the tube shows a tendency to decrease, which can be attributed to the increase in the vertical cross-sectional area at the tube's outlet. For the velocity cloud diagrams of the vertical cross-sections, the flow velocity is highest near the center of each section. The flow velocity distribution is more uniform in sections without a guided groove, whereas sections with a guided groove exhibit a greater velocity gradient. Notably, the velocity gradient near the lower guided-groove is more pronounced than that near the upper guided-groove, indicating that the curved segment of the lower guided-groove exerts a stronger adsorption effect on the seeds than the linear segment of the upper guided-groove. Furthermore, as the inlet flow velocity increases, the central flow velocity in each vertical cross-section also increases. Specifically, the central flow velocity in sections with a guided-groove trough reaches 68~75 m/s when the inlet velocity ranges from 60.64

to 63.48 m/s. In contrast, the flow velocity at the edge of the guided-groove trough remains largely unaffected by changes in inlet velocity, consistently ranging between 0 and 8 m/s.

It can be seen from Fig. 6 d that for the pressure cloud diagrams in the axial plane, the change of the velocity-inlet has a greater influence on the pressure gradient of the linear segments, and has a smaller influence on the pressure gradient of the curved segments. With the increase of the velocity-inlet, the pressure gradient range of the linear segment increases from 0~400Pa to 0~600Pa, while the area of the cloud of the curved segment, which only has a pressure gradient range of -300~-100Pa, exhibits a trend of gradual expansion. For the pressure maps of each vertical cross section, along with the increase of the velocity-inlet, the pressure distributions of the sections without guided-groove and the sections of upper guided-groove did not show obvious difference, but the sections of lower guided-groove showed an obvious pressure gradient evolution: the area of the maps with the pressure gradient range of -100~0Pa gradually decreased, while the area of the maps with the pressure gradient range of -300~-200Pa continued to increase. This indicates that increasing the velocity-inlet will obviously increase the pressure difference near the lower guided-groove, which will help to improve the stability and reliability of the seed guide tube in the process of seed-attracting and seed-attaching.

Results of the bench experiments

According to the range of factors in Table 2, the bench test was designed and conducted based on the central composite design, and the test results were obtained, as shown in Table 3.

Table 3

Results of the multi-factor experiments

Number.	Experimental factors		Experimental indexes	
	$X1$/ kPa	$X2$/ (km/h)	Q_1/ %	Q_2/ %
1	2.92	12.6	96.23	7.06
2	3.98	12.6	95.54	7.92
3	2.92	15.4	93.42	10.86
4	3.98	15.4	92.83	9.32
5	2.70	14.0	94.82	10.09
6	4.20	14.0	94.08	8.76
7	3.45	12.0	97.07	6.36
8	3.45	16.0	92.01	11.16
9	3.45	14.0	95.93	9.42
10	3.45	14.0	95.62	9.47
11	3.45	14.0	95.91	9.81
12	3.45	14.0	95.88	9.79
13	3.45	14.0	95.69	9.83

The results were processed and analysed using Design Expert 12 software, and the analysis of variance of the quadratic equation was obtained, as shown in Table 4.

Table 4

Analysis of variance of the quadratic equation

Source	Q_1				Q_2			
	Sum of squares	df	*F*-value	*p*-value	Sum of squares	df	*F*-value	*p*-value
Model	26.02	5	86.47	< 0.0001**	22.27	5	37.10	< 0.0001**
$X1$	0.6766	1	11.24	0.0122*	0.8198	1	6.83	0.0348*
$X2$	20.08	1	333.74	< 0.0001**	17.96	1	149.61	< 0.0001**
$X1\,X2$	0.0025	1	0.0415	0.8443	1.44	1	11.99	0.0105*
$X1^2$	3.17	1	52.75	0.0002**	0.2649	1	2.21	0.1811
$X2^2$	2.77	1	45.95	0.0003**	1.94	1	16.13	0.0051**
Residual	0.4213	7			0.8405	7		
Lack of fit	0.3415	3	5.71	0.0627	0.6786	3	5.59	0.0649
Pure error	0.0797	4			0.1619	4		
Cor total	26.44	12			23.11	12		

Note: * indicates a significant impact; ** indicates a highly significant impact.

In Table 4, the *p*-value of the regression model of the qualified index Q_1 and the coefficient of variation Q_2 were all less than 0.01, indicating that the regression model was highly significant, and the *p*-value of the lack of fit were all greater than 0.05 as non-significant, indicating that the regression model was well fitted.

In the analysis of variance of the Q_1, the $X2$, secondary terms $X1^2$ and $X2^2$ showed highly significant effects, the $X1$ showed significant effects, and interaction terms $X1X2$ showed insignificant effects. The magnitude of the effect of each factor on the Q_1 was $X2>X1$. After excluding the insignificant factors, the quadratic regression equation of the Q_1 was:

$$Q_1 = 23.00735 + 16.0239X1 + 7.7066X2 - 2.40178X1^2 - 0.31525X2^2 \qquad (19)$$

In the analysis of variance of the Q_2, the $X2$ and secondary terms $X2^2$ showed highly significant effects, the $X1$ and interaction term $X1X2$ showed significant effects, and secondary term $X1^2$ showed insignificant effects. The magnitude of the effect of each factor on the Q_2 was $X2>X1$. After excluding the insignificant factors, the quadratic regression equation of the Q_2 was:

$$Q_2 = -91.077 + 10.59639X1 + 10.85005X2 - 0.8X1X2 - 0.251087X2^2 \qquad (20)$$

Based on the results of the multi-factor experiment, the highest Q_1 and the lowest Q_2 are used as the optimization objectives, and the optimization equation is established within the factor range:

$$\left\{ \begin{array}{l} maxQ_1 \\ minQ_2 \\ s.t. \left\{ \begin{array}{l} 2.7\text{kPa} \geq X1 \geq 4.2\text{kPa} \\ 12\text{km/h} \geq X2 \geq 16\text{km/h} \\ 1 \geq Q_1(X1, X2) \geq 0 \\ 1 \geq Q_2(X1, X2) \geq 0 \end{array} \right. \end{array} \right. \qquad (21)$$

It was calculated that when the chamber pressure was 3.124 kPa and the operating speed was 12.0 km/h, the predicted values of the Q_1 and the Q_2 of the seed-guiding device were 96.709% and 6.08%, respectively. Under this parameter combination, 5 repetitive bench tests were carried out, and the results were shown in Table 5. At the same time, in order to check the performance improvement effect under this parameter combination compared with the traditional seed guide tube with guided-groove (Type B) and the seed guide tube without guided-groove based on the brachistochrone (Type C), five repetitive bench tests were carried out under the same conditions for these two types of seed guide tube, and the comparative results are shown in Table 5.

Table 5

Bench validation and comparative test results

Test number	Type of seed guide tube	Q_1/ %	Q_2/ %	Deviation from the Q_1 predicted value /%	Deviation from the Q_2 predicted value /%
	A	97.04	6.11	0.33	0.03
1	B	94.36	7.22	-2.35	1.14
	C	90.76	7.93	-5.95	1.85
	A	97.11	6.19	0.40	0.11
2	B	94.45	7.37	-2.26	1.29
	C	91.03	8.23	-5.68	2.15
	A	96.84	6.27	0.13	0.19
3	B	93.97	7.13	-2.74	1.05
	C	90.22	8.36	-6.49	2.28
	A	97.22	6.09	0.51	0.01
4	B	94.53	6.93	-2.18	0.85
	C	90.49	7.96	-6.22	1.88
	A	96.97	6.22	0.26	0.14
5	B	93.78	7.24	-2.93	1.16
	C	89.94	8.47	-6.77	2.39
	A	97.04±0.13	6.18±0.07	0.33	0.10
Statistical results	B	94.22±0.29	7.18±0.15	-2.49	1.10
	C	90.49±0.38	8.19±0.21	-6.22	2.11

Note: *A* indicates the seed guide tube with guided-groove based on the brachistochrone, *B* indicates the traditional seed guide tube with guided-groove, and *C* indicates the seed guide tube without guided-groove based on the brachistochrone.

In the table, the Q_1 and the Q_2 of the seed guide tube with guided-groove based on the brachistochrone (Type A) under the optimal parameter combination are 97.04±0.13% and 6.18±0.07%, 95% confidence Interval ≈ [96.88%, 97.20%] and 95% confidence Interval ≈ [6.09%, 6.27%], respectively, and the deviation of the results from the prediction is less than 0.4% with a relatively small error. This parameter combination further improves the seed-guiding performance of the seed-guiding device, which indicates that the results of the parameter optimization have a certain reliability. In addition, the Q_1 of the type A increased by 2.82% and 6.55%

compared with type B and C, and the Q_2 of the type A decreased by 1.00% and 2.01% compared with type B and C, which indicates that the seed guide tube with guided-groove based on the brachistochrone has a better seed-guiding performance. In addition, a high-speed camera was used in the experiment to measure the time for seeds to pass through type A, type B and type C as 0.029s, 0.035s and 0.033s, respectively, and the type A and type C were faster than the type B. This indicates that the seed guide tube designed based on the theory of the brachistochrone is able to shorten the time of the seed-guiding process effectively.

CONCLUSIONS

In order to improve the seeding quality of the planter for maize dense planting when it operates at high speed, a seed-guiding device with air-assisted and guided-groove is designed based on the principle of the brachistochrone. The flow field characteristics of the seed guide tube were investigated using CFD simulation. When the flow velocity at the inlet of the seed guide tube was 63.48, 60.64, 57.73, 54.69, 51.50, and 48.15 m/s, the flow velocity in the *y*-axis direction ranged from 36.87 to 56.23 m/s, 39.85 to 60.04 m/s, 42.71 to 63.66 m/s, 45.47 to 67.11 m/s, 48.13 to 70.41 m/s, and 50.72 to 73.63 m/s, respectively, and the maximum differential pressure was 484.11, 546.29, 608.66, 670.80, 732.73, and 795.78Pa, respectively. The two-factor and five-level central combination test was conducted under the conditions of 2.7~4.2 kPa of chamber pressure and 12~16 km/h of operating speed. The test results showed that the seed-guiding performance of the designed seed-guiding device was optimal under the parameter combinations of 3.124 kPa of chamber pressure and 12.0 km/h of operating speed, and the deviation between the results of the bench validation test and the results of the prediction was less than 0.4%. In addition, under the optimal parameter combination, the device's qualified index increased by 2.82% and 6.55%, and the coefficient of variation decreased by 1.00% and 2.01%, respectively, compared with that of the traditional seed guide tube with guided-groove and the seed guide tube without guided-groove based on the brachistochrone. This study shows that the combination of "airflow assisted + guided-groove structure + the brachistochrone" can effectively control the seed movement in the seed guide tube, and further improve the seeding uniformity and stability of the seed-guiding process of the maize delta-row dense planting planter under high-speed operating conditions.

ACKNOWLEDGEMENT

REFERENCES

[1]　Adetifa, B. O., & Aremu, A. K. (2021). Energy and exergy parameters of low-temperature solar thermal energy storage systems: empirical estimation and optimisation. *International Journal of Exergy*, Vol. 35, Issue 3, pp. 374-405. https://doi.org/10.1504/IJEX.2021.115904

[2]　Dong, J., Gao, X., Zhang, S., Huang, Y., Zhang, C., & Shi, J. (2023). Design and test of guiding seed throwing mechanism for maize posture control and driving metering device. *Transactions of the Chinese Society of Agricultural Machinery*, Vol. 54, Issue 10, pp. 25-34. https://doi.org/10.6041/j.issn.1000-1298.2023.10.002

[3]　Fanigliulo, R., Grilli, R., Benigni, S., Fornaciari, L., Biocca, M., & Pochi, D. (2022). Effect of sowing speed and width on spacing uniformity of precision seed drills. *INMATEH-Agricultural Engineering*, Vol. 66, Issue 1, pp. 9-18. https://doi.org/10.35633/inmateh-66-01

[4]　Jia, X., Zhu, J., Guo, G., Huang, Y., Gao, X., & Zhang, C. (2024). Design and test of a novel converging groove-guided seed tube for precision seeding of maize. *Biosystems Engineering*, Vol. 245, pp. 36-55. https://doi.org/10.1016/j.biosystemseng.2024.06.012

[5]　Li, X., Liao, Q., Wang, L., Li, M., & Du, W. (2023). Design and experiments of the type-hole wheel with high-speed air-assisted centralized metering device for rice, wheat and rapeseed. *Transactions of the Chinese Society of Agricultural Engineering*, Vol. 39, Issue 14, pp. 35-48. https://doi.org/10.11975/j.issn.1002-6819.202303044

[6]　Li, Y., Yang, L., Zhang, D., Cui, T., Zhang, K., Xie, C., & Yang, R. (2020). Analysis and test of linear seeding process of maize high speed precision metering device with air suction. *Transactions of the Chinese Society of Agricultural Engineering*, Vol. 36, Issue 9, pp. 26-35. https://doi.org/10.11975/j.issn.1002-6819.2020.09.003

[7] Liao, Y., Li, C., Liao, Q., & Wang, L. (2020). Research progress of seed guiding technology and device of planter. *Transactions of the Chinese Society of Agricultural Machinery*, Vol. 51, Issue 12, pp. 1-14. https://doi.org/10.6041/j.issn.1000-1298.2020.12. 001

[8] Liu, R., Liu, Y., Liu, Z., & Liu, L. (2023). Research on positive pressure airflow assisted blowing and seed guiding device of corn high-speed precision planter. *Transactions of the Chinese Society of Agricultural Machinery*, Vol. 54, Issue 7, pp. 156-166. https://doi.org/10.6041/j.issn.1000-1298.2023.07.015

[9] Ma, C., Yi, S., Tao, G., Li, Y., Wang, S., Wang, G., & Gao, F. (2023). Research on receiving seeds performance of belt-type high-speed corn seed guiding device based on discrete element method. *Agriculture*, Vol. 13, Issue 5, pp. 1085. https://doi.org/10.3390/agriculture13051085

[10] Sun, W., Yi, S., Qi, H., Dai, Z., Zhang, Y., & Wang, S. (2024). Research progress on narrow row and dense planting delta-row seeding technology and equipment. *Agricultural Engineering*, Vol. 14, Issue 5, pp. 5-9. https://doi.org/10.19998/j.cnki.2095-1795.2024.05.001

[11] Sun, W., Yi, S., Qi, H., Li, Y., Dai, Z., Zhang, Y., & Wang, S. (2024). Design and experiment of progressive seed-cleaning mechanism for air-pressure maize precision seed-metering device. *INMATEH-Agricultural Engineering*, Vol. 73, Issue 2, pp. 473-486. https://doi.org/10.35633/inmateh-73-40

[12] Sun, W., Yi, S., Qi, H., Wang, S., Li, Y., & Dai, Z. (2024). Design and experiment of twin discs intertwined air-pressure high-speed precision seed-metering device for maize delta-row dense plantings. *Transactions of the Chinese Society of Agricultural Machinery*, Vol. 55, Issue 10, pp. 168-179. https://doi.org/10.6041/j.issn.1000-1298.2024.10.016

[13] Tang, H., Guan, T., Xu, F., Xu, C., & Wang, J. (2024). Test on adsorption posture and seeding performance of the high-speed precision dual-chamber maize metering device based on the seed characteristics. *Computers and Electronics in Agriculture*, Vol. 216, pp.108471. https://doi.org/10.1016/j.compag.2023.108471

[14] Tang, H., Xu, F., Guan, T., Xu, C., & Wang, J. (2023). Design and test of a pneumatic type of high-speed maize precision seed metering device. *Computers and Electronics in Agriculture*, Vol. 211, pp.107997. https://doi.org/10.1016/j.compag.2023.107997

[15] Tang, H., Xu, F., Xu, C., Zhao, J., & Wang, Y. J. (2023). The influence of a seed drop tube of the inside-filling air-blowing precision seed-metering device on seeding quality. *Computers and Electronics in Agriculture*, Vol. 204, pp.107555. https://doi.org/10.1016/j.compag.2022.107555

[16] Yatskul, A., & Lemiere, J.P. (2018). Establishing the conveying parameters required for the air-seeders. *Biosystems Engineering*, Vol. 166, pp. 1-12. https://doi.org/10.1016/j.biosystemseng.2017.11.001

[17] Yi, S., Zhang, Y., Dai, Z., Kong, L., Sun, W., & Xu, L. (2025). Design and experiment of positive pressure airflow guide groove seed guiding device for maize delta-row high-speed precision seeder. *Transactions of the Chinese Society of Agricultural Machinery*, Vol.56, Issue 2, pp. 261-274. https://doi.org/10.6041/j.issn.1000-1298.2025.02.025

[18] Zhao, P., Gao, X., Su, Y., Xu, Y., & Huang, Y. (2024). Investigation of seeding performance of a novel high-speed precision seed metering device based on numerical simulation and high-speed camera. *Computers and Electronics in Agriculture*, Vol. 217, pp.108563. https://doi.org/10.1016/j.compag.2023.108563